nature physics

ARTICLES

PUBLISHED ONLINE: 30 MARCH 2014 | DOI: 10.1038/NPHYS2924

Ferroelectric quantum criticality

S. E. Rowley[1,2,3*], L. J. Spalek[1†], R. P. Smith[1], M. P. M. Dean[1‡], M. Itoh[4], J. F. Scott[1], G. G. Lonzarich[1*] and S. S. Saxena[1,5*]

Paramagnets on the border of ferromagnetism at low temperatures are more subtle and complex than anticipated by the conventional theory of quantum critical phenomena. Could quantum criticality theory be more relevant in the corresponding case of quantum paraelectrics on the border of ferroelectricity? To address this question we have investigated the temperature dependence of the dielectric function of the displacive quantum paraelectrics $SrTiO_3$, oxygen-18 substituted $SrTiO_3$ and $KTaO_3$. In all of these materials on the border of ferroelectricity we observe non-classical T^2 temperature dependencies of the inverse dielectric function below 50 K, followed by anomalous upturns below a few kelvin extending into the millikelvin range. This non-classical behaviour can be understood quantitatively without adjustable parameters in terms of quantum criticality theory when extended to include the effects of long-range dipolar interactions and the coupling of the electric polarization field with acoustic phonons. The quantum critical regime in displacive ferroelectrics is thus strikingly different from that in the better-known ferromagnetic counterparts and offers unexpected prospects in the field of quantum phase transitions.

The study of classical critical phenomena has led to the development of a number of fruitful concepts of surprisingly far-reaching relevance in science. The corresponding study of the quantum analogue of critical phenomena might be expected to be no less important. However, in practice, quantum critical behaviour can be masked by the occurrence of first-order quantum phase transitions or the emergence of unexpected or exotic forms of quantum order (for example, refs 1–6). Examples of such complicating but intriguing effects on the border of metallic ferromagnetism at low temperature are given in Fig. 1. Despite extensive searches over the past few decades, simple examples of quantum critical behaviour have been difficult to find. Notable exceptions would seem to include certain frustrated layered magnetic insulators that exhibit field-tuned transitions between paramagnetic to antiferromagnetic states accompanied by subtle forms of dimensional reduction[7–10]. In this Article we show that certain materials on the border of ferroelectric order at low temperatures, namely certain displacive quantum paraelectrics[11], exhibit quantum criticality uninterrupted over a wide temperature range by either first-order transitions or new forms of quantum order that seem to be ubiquitous in the corresponding quantum paramagnetic systems of the kind illustrated by Fig. 1.

The ferroelectrics differ from quantum magnets in a number of ways and have traditionally formed independent subjects of study (Table 1). In particular, the ferroelectrics described here exhibit transitions between homogeneous states without the application of symmetry breaking fields and do not involve the complication of dimensional reduction. The effective dimension in the quantum critical description is intriguingly the marginal dimension of three plus one, that is, three space dimensions plus one time dimension as is the case in elementary particle physics, rather than three plus two or two plus two as in the above quantum magnets. Furthermore, the electric dipoles in ferroelectrics do not exhibit quantum precession phenomena, which can lead in principle to subtle effects in spin systems[1,12]. These effects are described by non-trivial terms in the effective action of a kind that interestingly do not arise in the ferroelectrics. Finally, we note that ferroelectrics offer the possibility of electric field rather than magnetic field tuning for certain applications, such as in solid-state refrigeration technologies and tuning of carrier concentrations for the control of superconducting and other properties[13,14].

Early descriptions of critical phenomena on the border of continuous phase transitions in the limit of absolute zero were based on ϕ^4-quantum field models (for example, refs 15–17 for the case of quantum paraelectrics and ref. 1 more generally). They differ from the Ginzburg–Landau–Wilson models of classical critical phenomena by the inclusion of the dynamics of the order parameter field $\phi(r, \tau)$, which can represent a coarse-grained magnetic or electric polarization as a function of the spatial coordinate r and temporal coordinate τ. In quantum statistical mechanics, τ is an imaginary time that has a finite range at non-zero temperature, $0 < \tau < \hbar/(k_B T)$ (ref. 1). This approach leads to a model of critical phenomena with both spatial and temporal dimensions. The effective dimension for quantum criticality can be taken to be $d_{\mathrm{eff}} = d + z$, where d is the spatial dimension and z is the dynamical exponent defined by the dispersion relation, $\omega_q \sim q^z$, that is, the wavevector dependence of the frequency spectrum ω_q of fluctuations of the order parameter field at a small wavevector q.

In this description, quantum critical behaviour is analogous to the classical counterpart, but in a higher dimension; importantly, the temporal dimension is of a finite size, which is determined by the temperature. An intriguing consequence of this higher dimensionality is that the self-consistent field approximation of the ϕ^4-field model, which is not strictly applicable in the classical limit in normal materials near to the critical point, might be relevant in the quantum limit if d_{eff} is not below four, that is, in three spatial

[1]Cavendish Laboratory, University of Cambridge, J.J. Thomson Avenue, Cambridge, CB3 0HE, UK, [2]Department of Physics, Princeton University, Princeton, New Jersey 08544, USA, [3]Centro Brasileiro de Pesquisas Físicas, Rua Dr Xavier Sigaud 150, Rio de Janeiro, 22290-180, Brazil, [4]Materials & Structures Laboratory, Tokyo Institute of Technology, 4259 Nagatsuta, Midori, Yokohama 226-8503, Japan, [5]Centre for High Technologies, 3a, University Street, Olmazor District, Tashkent, 100174, Uzbekistan. †Current address: Academic Centre for Materials and Nanotechnology, AGH University of Science and Technology, Krakow, Poland. ‡Current address: Condensed Matter Physics and Materials Science Department, Brookhaven National Laboratory, Upton, New York, 11973, USA. * e-mail: ser41@cam.ac.uk; gl238@cam.ac.uk; sss21@cam.ac.uk

Table 1 | Comparison of electric and magnetic dipole systems.

	Ferroelectric materials	Ferromagnetic materials
Origin of dipole	Charge separation (no intrinsic angular momentum)	Charge flow (intrinsic spin angular momentum)
Dipole interaction	Coulomb (strong)	Ampere (weak relativistic)
Short-range interaction	Elastic coupling	Exchange coupling
Origin of anisotropy	Crystal electric fields	Spin-orbit coupling
Phase transitions	Often first order, non-mean field behaviour rare	Often second order, non-mean field behaviour observed
Dynamics	Generally propagating atomic vibrations	Precessional and dissipative spin fluctuations
Tuning parameter	Electric field (voltage gating)	Magnetic field

Despite seeming similar, electric and magnetic dipole systems in fact exhibit important differences.

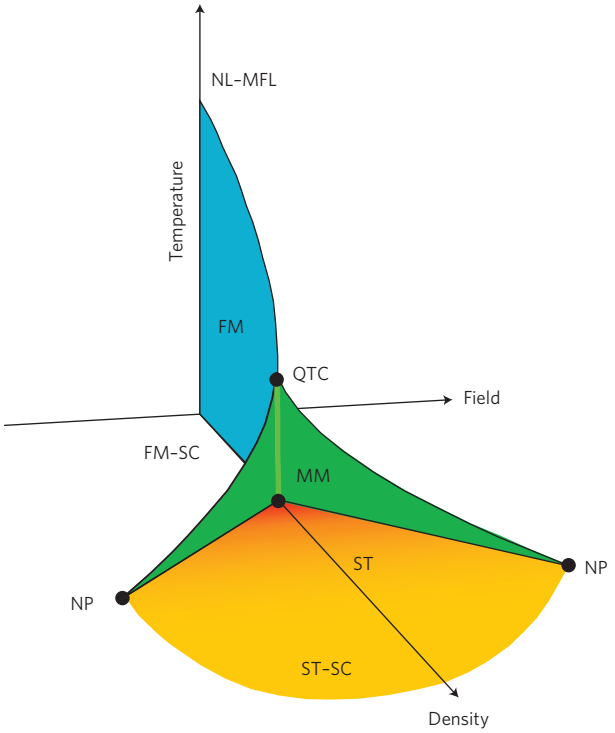

Figure 1 | Temperature–magnetic field–density phase diagram on the border of metallic ferromagnetism. Qualitative form of the phase diagram predicted in a quantum Ginzburg–Landau–Wilson model with an attractive mode–mode coupling term (attractive ϕ^4 term) in the low-temperature limit. With increasing density, or applied pressure, a second-order ferromagnetic transition line bifurcates at a tricritical point into two sheets of first-order metamagnetic transitions. Selected examples of phenomena observed on the border of metallic ferromagnetism (FM) and metamagnetism (MM) are indicated (ref. 6): NL-MFL = non-local marginal Fermi liquid in $ZrZn_2$; FM-SC = ferromagnetism and superconductivity in UGe_2; QTC = quantum tri-criticality in Ni_3Ga; ST = spin texture (skyrmions) in MnSi; ST-SC = spin-triplet superconductivity on the border of ferromagnetism in M_2RuO_4 (M stands for Sr or Ca) and NP = electron nematic phase in $Sr_3Ru_2O_7$.

Table 2 | Quantum criticality on the border of displacive ferroelectricity and metallic ferromagnetism.

	Displacive ferroelectric quantum critical point*	Metallic ferromagnetic quantum critical point†
Fluctuation spectrum	$\omega_q \propto (\kappa^2+q^2)^{1/2}$	$\Gamma_q \propto q\,(\kappa^2+q^2)$
$z(\kappa \to 0)$	1	3
$d_{\rm eff}$	4	6
$\chi(T)$	$1/T^2$	$1/T^{4/3}$

The table presents the dispersion relation ω_q versus wavevector q, dynamical exponent z, effective dimension $d_{\rm eff} = d + z$, and quantum critical exponent of the order parameter susceptibility $\chi(T)$, in the self-consistent-field approximation to the quantum ϕ^4-field model for a multiaxial displacive ferroelectric and for a metallic ferromagnet in three dimensions ($d = 3$). The self-consistent field approximation is expected to be qualitatively correct for $d_{\rm eff} > 4$ and predicts $\chi(T) \sim 1/T^{\gamma}$, where $\gamma = (d_{\rm eff} - 2)/z$ at the quantum critical point. In the dispersion relation, κ is a correlation wavevector that vanishes at the quantum critical point. The fluctuation spectrum for an itinerant-electron ferromagnet is characterized by a relaxation rate Γ_q versus q. The origin of the above non-classical temperature dependence of $\chi(T)$ is discussed in the Supplementary Information. *A logarithmic correction to $\chi(T)$ is expected, as in this case $d_{\rm eff}$ is equal to the upper critical dimension. †Excluding non-analytical corrections arising from transverse magnetic fluctuations.

dimensions if the dynamical exponent is not less than unity. A weakly varying logarithmic correction to the self-consistent field approximation that arises for the case of the marginal dimension, $d_{\rm eff} = 4$ (refs 17 and 18), will be discussed below.

The predictions of the above quantum criticality model in the self-consistent field approximation are compared and contrasted for simple systems on the border of metallic ferromagnetism and displacive ferroelectricity in Table 2. The results are for three spatial dimensions in the absence of frozen-in disorder. A dynamical exponent of three for the border of metallic ferromagnetism is that predicted by the self-consistent-renormalization model (ref. 6 and references therein). This leads to an effective dimension, $d_{\rm eff}$, of six and a critical exponent of 4/3 for the inverse magnetic susceptibility, that is, $1/\chi(T) \sim T^{4/3}$. A dynamical exponent of unity on the border of displacive ferroelectricity is that predicted by the self-consistent-phonon model in the limit of a vanishing gap of the transverse optical mode[15–17,19–28]. This leads to an effective dimension of four and thus a critical exponent for the inverse susceptibility of essentially two, that is, $1/\chi(T) \sim T^2$.

Interestingly, the predicted behaviour for the temperature dependence of $1/\chi(T)$ on the border of metallic ferromagnetism has not been unambiguously observed. The breakdown of the quantum criticality model in this case may be attributed in general to the emergence of first-order transitions and a multiplicity of quantum critical fields (see Fig. 1 and references cited in the accompanying caption). These effects may be traced back, at least in part, to the existence of a high density of gapless electron–hole excitations on the Fermi surface, which is a chief characteristic of the metallic state.

The theory of quantum criticality might be expected to have greater relevance to the case of ferroelectricity in semiconductors or insulators in which electron–hole excitations are fully gapped and their role at low temperatures limited to a straightforward renormalization of the parameters in the ϕ^4-quantum field description. This simplification could be offset by a new

complication, namely, the presence of the long-range dipole–dipole interaction that can be several orders of magnitude stronger than that in the corresponding ferromagnetic materials, in which the dipole–dipole interaction is relativistic. A number of analyses have shown, however, that the long-range interaction leads principally to a suppression of longitudinal fluctuations of the electric polarization, that is, fluctuations in the component of the order parameter field parallel to the wavevector, which lead to fluctuations of the bound charge density and thus to high excitation energies[16,18,22,29–33]. As in the case of gapped electron–hole excitations, the role of the dipolar interaction is thus to renormalize the parameters of the ϕ^4-quantum field model, in which only transverse polarization fluctuations are critical, that is, gapless (at the centre of the Brillouin zone) in the quantum critical regime.

The applicability of the ϕ^4-quantum field model in the self-consistent field approximation might also fail in the case of quantum paraelectrics as a result of other effects, including the presence of marginal dimensionality[17,22] ($d_{\mathrm{eff}} = 4$ in a cubic material) and the coupling of the order parameter field to the strain field—that is, to acoustic phonons[16,26]. Despite these potential complexities, and in contrast to the behaviour observed on the border of metallic ferromagnetism, we find that the ϕ^4-quantum field model in the self-consistent field approximation is relevant to the displacive quantum paraelectrics $SrTiO_3$, oxygen-18 substituted $SrTiO_3$ and $KTaO_3$ that crystallize in the cubic perovskite structure at room temperature and for which d is essentially three (Supplementary Information).

In particular, as shown in Figs 2a and 3a, the inverse dielectric function, $1/\varepsilon(T)$, which essentially equals $1/\chi(T)$ under our conditions, exhibits the predicted non-classical T^2 temperature dependence over a wide range below approximately 50 K. The T^2 regime is wider, as expected, in the material with the higher dielectric function in the limit of absolute zero, namely, in $SrTiO_3$, which is closer to the ferroelectric quantum phase transition than $KTaO_3$. The T^2 variation is expected to cross over to an exponential form at very low temperatures if the gap of the transverse optical mode does not vanish. As shown in the lower insets of Figs 2a and 3a, the inverse dielectric functions instead exhibit shallow minima and upturns that extend into the millikelvin range. This behaviour is qualitatively of the form expected from the effects of the above-mentioned coupling of the order parameter field with acoustic phonons, namely, the electrostrictive effect[16,26].

To check that the origins of the T^2 temperature variation and low-temperature upturn of the inverse dielectric function have been correctly identified, we have carried out a numerical calculation of the prediction of the ϕ^4-quantum field model extended to include the coupling of ϕ with the lattice strain field, that is, with acoustic phonons. The parameters of the model were not adjusted to fit the temperature variation, but were instead determined from independent measurements in the low-temperature limit. The magnitudes of the parameters and the way in which they were determined are presented in Supplementary Table I and the accompanying caption. The parameters are independent of temperature and the temperature variation of the dielectric function is determined entirely through the ϕ^4-quantum field model itself, in the self-consistent field approximation. The results shown in Figs 2b and 3b are sufficiently similar to the experimental results in Figs 2a and 3a to suggest that the origin of the T^2 variations and low-temperature upturns in the inverse dielectric function have been correctly identified. A schematic of the expected dimensionless temperature–pressure phase diagram for the parameters relevant to $SrTiO_3$ is shown in Fig. 4.

Long-range ferroelectric order can be induced in $SrTiO_3$ at low temperatures by the substitution of ^{16}O by the isotope ^{18}O, with a maximum Curie temperature of approximately 25 K in fully substituted crystals[34,35]. By varying the ^{18}O content we tuned single

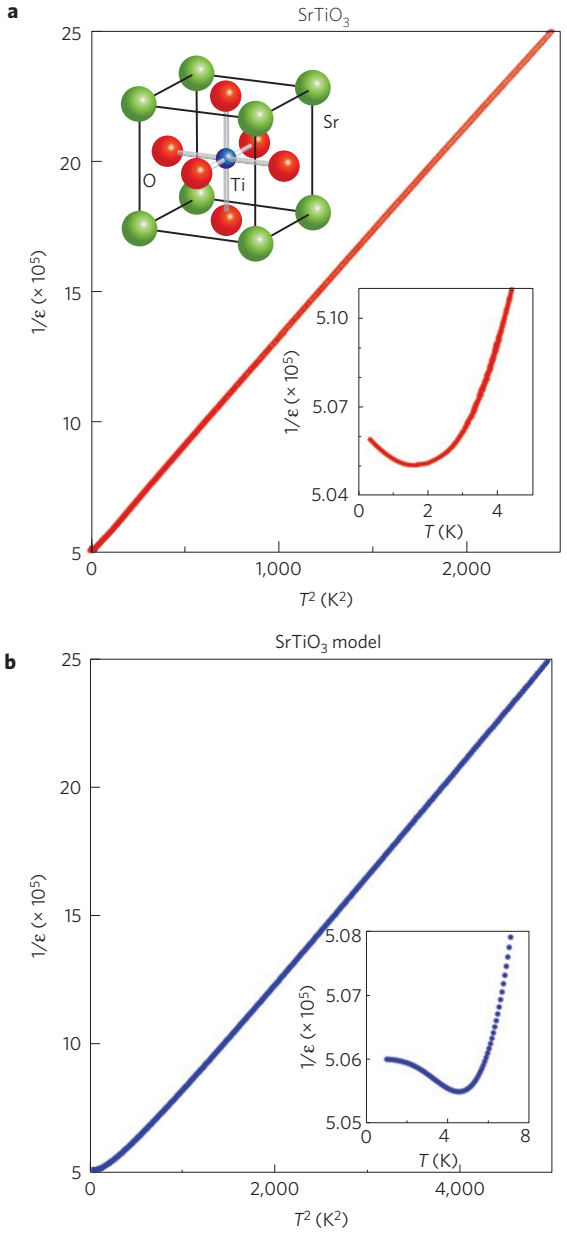

Figure 2 | Temperature dependence of the inverse dielectric function $1/\varepsilon(T)$ in $SrTiO_3$. **a**, Measured inverse dielectric function plotted against the square of the temperature up to approximately 50 K. The lower inset is an expanded view at low temperature, which exhibits an upturn below 4 K, measured with high precision[43,44]. The upper inset illustrates the unit cell of $SrTiO_3$ in its room-temperature cubic perovskite structure. **b**, Calculated inverse dielectric function in the quantum criticality model described in the text and Supplementary Information. The basic model parameters are given in Supplementary Table I. The dimensionless electrostrictive coupling parameter λ and velocity ratio η, defined in Supplementary Information, are approximately 0.03 (ref. 45) and 2 (ref. 46), respectively.

crystals of $SrTiO_3$ through its quantum critical point and measured the evolution of the temperature dependence of the inverse dielectric function (Fig. 5). The results are once again quantitatively consistent with the predictions of the quantum criticality model described here without the use of adjustable parameters (Fig. 5 insets). We have also considered the effect of quenched disorder, which inevitably arises in the preparation of sintered or doped samples. As shown in Supplementary Fig. I, the non-classical T^2 temperature dependence of the inverse dielectric function in $SrTiO_3$ is a robust phenomenon

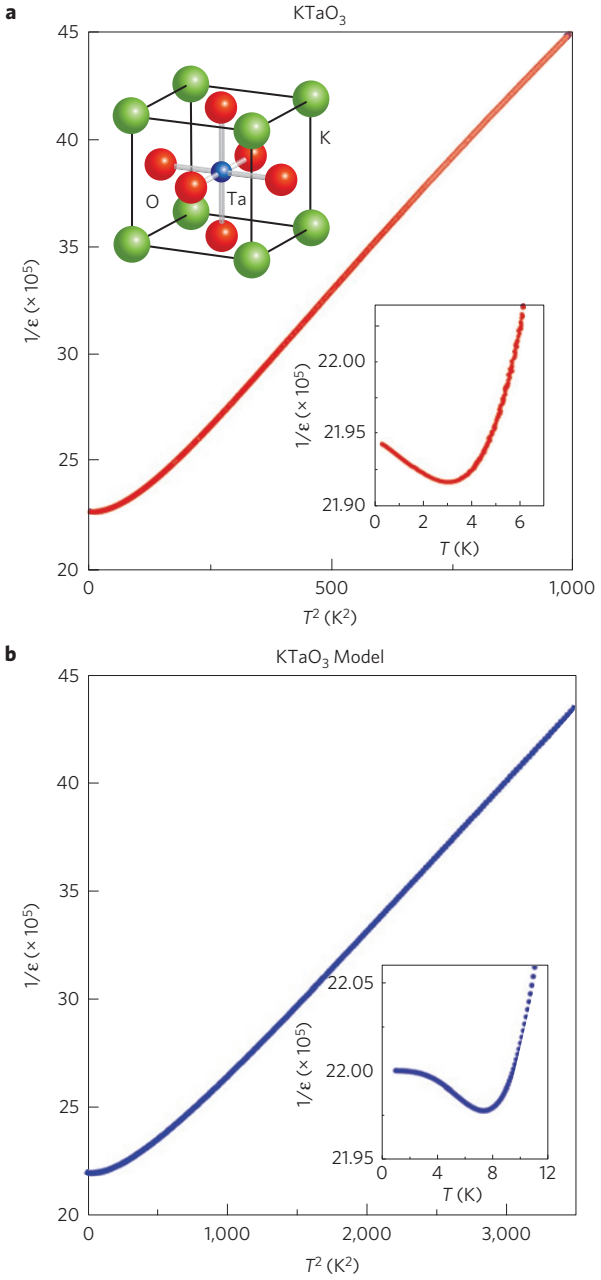

Figure 3 | Temperature dependence of the inverse dielectric function $1/\varepsilon(T)$ in $KTaO_3$. **a**, Measured inverse dielectric function plotted against the square of the temperature. The lower inset is an expanded view at low temperature, which exhibits an upturn below 4 K. The upper inset illustrates the unit cell of $KTaO_3$ in its cubic perovskite structure. **b**, Calculated inverse dielectric function in the quantum criticality model described in the text and Supplementary Information. The basic model parameters are given in Supplementary Table I. The dimensionless electrostrictive coupling parameter λ and velocity ratio η, defined in Supplementary Information, are approximately 0.02 (ref. 47) and 2 (ref. 48), respectively.

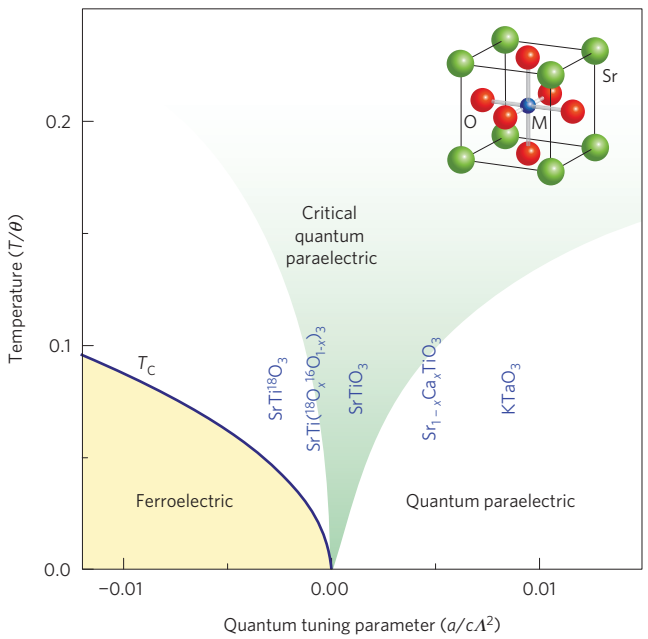

Figure 4 | Phase diagram for a displacive ferroelectric. The phase diagram is based on the quantum ϕ^4-field model described in the text and defined more fully in Supplementary Information. It is characterized by four model parameters, three of which, a, b and c, are defined by the $T=0$ static equation of state $\varepsilon_0 E = aP + bP^3 - c\nabla^2 P$, where E is the electric field and P is the polarization, and the fourth parameter, v, is the sound velocity for the critical transverse optical mode. The vertical axis is the temperature normalized to the effective Debye temperature $\theta = \hbar v \Lambda / k_B$, where Λ is the Debye wavevector, while the horizontal axis is the ratio a/c normalized to Λ^2. For positive values of a, the ratio a/c corresponds to the square of the zero-temperature correlation wavevector, which vanishes at the quantum critical point separating the ferroelectric and paraelectric states at absolute zero. The quantum tuning parameter can be varied, for example, by the application of hydrostatic pressure, by isotopic substitution as in the case of $SrTi(^{18}O_x^{16}O_{1-x})_3$, or by chemical substitution as in the case of $Sr_{1-x}Ca_xTiO_3$. The calculations are based on the parameters for $SrTiO_3$ (Supplementary Information) for both positive and negative values of the parameter a. The shading highlights the expected critical quantum paraelectric regime characterized by an approximately quadratic temperature dependence of the inverse dielectric function, as seen in $SrTiO_3$, the ^{18}O substituted $SrTiO_3$ and $KTaO_3$ (Figs 2, 3 and 5). The crossover from the low-temperature T^2 behaviour to the high-temperature classical behaviour arises at temperatures on the order of 50 K–100 K in all of the above materials in both the model calculations and experiment. As explained in Supplementary Information, in the low-temperature limit and as a tends to zero, the T^2 inverse dielectric function (more precisely, the inverse susceptibility) and the Curie temperature may be expressed in terms of the basic model parameters in the closed forms: $\chi^{-1} = a + (5\varepsilon_0 k_B^2 b/(18\hbar c v))T^2$ and $k_B T_C = \sqrt{18\hbar c v\,|a|/(5\varepsilon_0 b)}$, respectively. We note that the low-temperature limit for $\chi(T)$ near to the ferroelectric quantum critical point is very different from that predicted by the Barrett formula sometimes used to describe quantum paraelectrics. The range of applicability of the Barrett formula, which is not applicable near to a ferroelectric quantum critical point, is discussed in Supplementary Information.

that is relatively insensitive to the kind of disorder that arises from the effects of sintering.

Other possible causes for the anomalous minima in the inverse dielectric function of pure $SrTiO_3$ and $KTaO_3$ have also been considered. In particular, the role of frozen-in disorder seems to be ruled out by the relative insensitivity of the position and depth of the minima to sample purity and measurement frequency (Supplementary Information). The role of residual dipole–dipole interactions beyond those already discussed[28] is estimated in terms of realistic parameters to be less important than that of the coupling to acoustic phonons. Finally, logarithmic corrections at the marginal dimension (three plus one in our case; refs 17,22) are not expected to produce a minimum in $1/\varepsilon(T)$, and numerical analyses predict

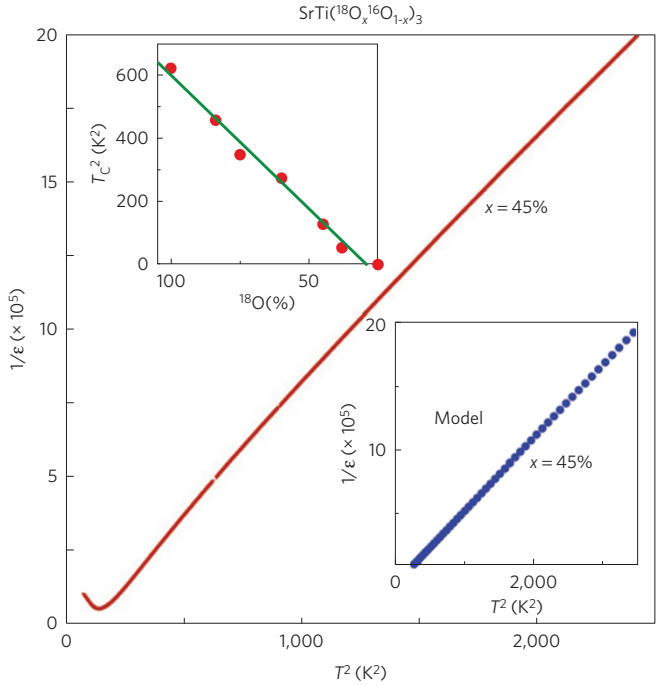

Figure 5 | Temperature dependence of the inverse dielectric function $1/\varepsilon(T)$ in $SrTi(^{18}O_x^{16}O_{1-x})_3$. The main figure gives an example of the observed inverse dielectric function versus the square of the temperature up to approximately 50 K for an intermediate value of x ($x=0.45$). The upper inset presents the square of the Curie temperature, T_C, versus x over the entire range $0<x<1$ (also ref. 34). The solid line in the upper inset is the prediction of the model presented in the text (Supplementary Information) with the parameter set (b, c, ν) for $x=0$ that can be inferred from Supplementary Table I, and the value of a varying linearly with x. The solid line is defined by the two conditions $x\approx 1/3$ at $a=0$ (where $T_C=0$) and $a\approx -7\times10^{-5}$ at $x=1$. This value of a at $x=1$ is consistent with estimates in the range from -5×10^{-5} to -10×10^{-5} inferred from our dielectric constant measurements[24] and those of the optical gap[49,50] for $SrTi^{18}O_3$, in the low-temperature limit. Lower insert: prediction of the quantum criticality model as in Fig. 1, but based on the above parameters and excluding the electrostrictive effect.

that they are unobservably weak under our experimental conditions. The logarithmic correction and effects of electrostriction beyond those considered here could lead to an attractive coupling of critical modes and a first-order transition very close to the ferroelectric quantum phase transition (Supplementary Information). This effect might be suppressed by quenched disorder arising, for example, in specimens in which quantum tuning is achieved by chemical or isotopic substitution. To minimize this problem in the case of isotopic substitution, ^{16}O might be replaced entirely by ^{18}O to produce a homogeneous ferroelectric with a starting transition temperature of approximately 25 K that can be tuned to zero without introducing quenched disorder by the application of hydrostatic pressure[34,36].

In summary, we find that, in contrast to the border of metallic ferromagnetism, the border of displacive ferroelectricity can exhibit an elementary form of quantum critical phenomena that can be understood in terms of a quantum generalization of the Ginzburg–Landau–Wilson theory over a wide temperature range. The mysterious upturn in the inverse dielectric function at very low temperatures can be understood within the same theory, extended to include the electrostrictive effect. This constitutes the first such description of the quantum regime on the border of ferroelectricity in terms of independently measured temperature-independent model parameters.

Finally, we note that the non-classical behaviour of a critical quantum paraelectric may be relevant to understanding related phenomena in other systems, perhaps including supersolids, which remain enigmatic[37,38]. The phase diagrams on the border of ferroelectric quantum critical points in general are likely to show, on still closer examination than presented here, some of the complexities depicted in Fig. 1. First-order transitions and tri-critical points are not infrequently observed in ferroelectrics, and indications of non-trivial textured states have been reported. The high dielectric constant of $SrTiO_3$ is thought to play a role in the formation of an unusual kind of superconductivity when carriers are introduced by chemical doping[39–41], ionic liquid gating[13], or other means[42]. Pairing seems to arise in the intriguing anti-adiabatic regime at low densities, where the Fermi energy of the itinerant carriers is much lower than the characteristic energies of the phonons believed to mediate the electron–electron attraction. The recent discoveries of superconductivity in gated $SrTiO_3$ (ref. 13) and $KTaO_3$ (ref. 14), in particular, are leading to a re-examination of the non-BCS anti-adiabatic regime that continues to pose a major challenge to theory.

Received 04 January 2013; accepted 14 February 2014; published online 30 March 2014

References

1. Sachdev, S. *Quantum Phase Transitions* (Cambridge Univ. Press, 1999).
2. Focus on quantum phase transitions. *Nature Phys.* **4,** 167–204 (2008).
3. Anderson, P. W. In praise of unstable fixed points: The way things actually work. *Physica B* **318,** 28–32 (2002).
4. Fradkin, E. & Kivelson, S. Electron nematic phases proliferate. *Science* **327,** 155–156 (2010).
5. Monthoux, P., Pines, D. & Lonzarich, G. G. Superconductivity without phonons. *Nature* **450,** 1177–1183 (2007).
6. Rowley, S. E. *et al.* Novel metallic states at low temperatures. *Low Temp. Phys.* **37,** 2–7 (2011).
7. Batista, C. *et al.* Geometric frustration and dimensional reduction at a quantum critical point. *Phys. Rev. Lett.* **98,** 257201 (2007).
8. Jaime, M. *et al.* Magnetic-field-induced condensation of triplons in Han Purple pigment $BaCuSi_2O_6$. *Phys. Rev. Lett.* **93,** 087203 (2004).
9. Giamarchi, T., Rüegg, C. & Tchernyshyov, O. Bose–Einstein condensation in magnetic insulators. *Nature Phys.* **4,** 198–204 (2008).
10. Kraemer, C. *et al.* Dipolar antiferromagnetism and quantum criticality in $LiErF_4$. *Science* **336,** 1416–1419 (2012).
11. Muller, K. A. & Burkard, H. $SrTiO_3$: Intrinsic quantum para-electric below 4 K. *Phys. Rev. B* **19,** 3593–3602 (1979).
12. Lonzarich, G. G. *Electron: A Centenary Volume, Ch. 6* (Cambridge Univ. Press, 1997).
13. Ueno, K. *et al.* Electric-field-induced superconductivity in an insulator. *Nature Mater.* **7,** 855–858 (2008).
14. Kawasaki, M. *et al.* Discovery of superconductivity in $KTaO_3$ by electrostatic carrier doping. *Nature Nanotech.* **6,** 408–412 (2011).
15. Rechester, A. B. Contribution to the theory of second-order phase transitions at low temperatures. *Sov. Phys. JETP* **33,** 423–430 (1971).
16. Khmelnitskii, D. E. & Shneerson, V. L. Low-temperature displacement-type phase transition in crystals. *Sov. Phys. Solid State* **13,** 687 (1971).
17. Khmelnitskii, D. E. & Shneerson, V. L. Phase transition of the displacement type in crystals at very low temperature. *Sov. Phys. JETP* **37,** 164–170 (1973).
18. Larkin, A. I. & Khmelnitskii, D. E. Phase transition in uniaxial ferroelectrics. *Sov. Phys. JETP* **29,** 1123–1128 (1969).
19. Schneider, T., Beck, H. & Stoll, E. Quantum effects in an n-component vector model for structural phase-transitions. *Phys. Rev. B* **13,** 1123–1130 (1976).
20. Bilz, H., Benedek, G. & Bussmann-Holder, A. Theory of ferroelectricity—the polarizability model. *Phys. Rev. B* **35,** 4840–4849 (1987).
21. Kvyatkovskii, O. E. Quantum effects in incipient and low-temperature ferroelectrics (a review). *Phys. Solid State* **43,** 1401–1419 (2001).
22. Roussev, R. & Millis, A. J. Theory of the quantum paraelectric–ferroelectric transition. *Phys. Rev. B* **67,** 014105 (2003).
23. Coleman, P. Theory perspective: SCES '05 Vienna. *Physica B* **378–80,** 1160–1169 (2006).
24. Rowley, S. E. *Quantum Phase Transitions in Ferroelectrics*, Ph.D. thesis, (Univ. Cambridge, 2010).
25. Rowley, S. *et al.* Ferromagnetic and ferroelectric quantum phase transitions. *Phys. Status Solidi B* **247,** 469–475 (2010).

26. Palova, L., Chandra, P. & Coleman, P. Quantum critical paraelectrics and the Casimir effect in time. *Phys. Rev. B* **79,** 075101 (2009).
27. Das, N. & Mishra, S. G. Fluctuations and criticality in quantum paraelectrics. *J. Phys. Conden. Mater.* **21,** 095901 (2009).
28. Conduit, G. J. & Simons, B. D. Theory of quantum paraelectrics and the metaelectric transition. *Phys. Rev. B* **81,** 024102 (2010).
29. Aharony, A. & Fisher, M. E. Critical behavior of magnets with dipolar interactions. I Renormalization group near four dimensions. *Phys. Rev. B* **8,** 3323–3341 (1973).
30. Lines, M. E. & Glass, A. M. *Principles and Applications of Ferroelectrics and Related Materials* (Clarendon, 2001).
31. Strukov, B. A. & Levanyuk, A. P. *Ferroelectric Phenomena in Crystals: Physical Foundations* (Springer, 1998).
32. Anderson, P. W. *Conf. Proc., Lebedev Physics Inst. USSR Acad of Sci. Fizika Dielektrikov* (*Moscow*) 290–297 (Nova Science Publishers, 1960).
33. Cochran, W. Crystal stability and the theory of ferroelectricity. *Adv. Phys.* **9,** 387–423 (1960).
34. Wang, R. & Itoh, M. Suppression of the quantum fluctuation in ^{18}O-enriched strontium titanate. *Phys. Rev. B* **64,** 174104 (2001).
35. Itoh, M. & Wang, R. P. Quantum ferroelectricity in $SrTiO_3$ induced by oxygen isotope exchange. *Appl. Phys. Lett.* **76,** 221–223 (2000).
36. Venturini, E. L., Samara, G. A., Itoh, M. & Wang, R. Pressure as a probe of the physics of ^{18}O-substituted $SrTiO_3$. *Phys. Rev. B* **69,** 184105 (2004).
37. Anderson, P. W. Bose fluids above T_c: Incompressible vortex fluids and 'supersolidity'. *Phys. Rev. Lett.* **100,** 215301 (2008).
38. Kubota, M., Shimizu, N., Yasuta, Y., Kitamura, A. & Yagi, M. Transition into the supersolid (SS) state, supersolid density ρ_{ss} and the critical velocity V_c to destroy the SS state. *J. Low Temp. Phys.* **162,** 483–491 (2011).
39. Schooley, J. F. *et al.* Dependence of the superconducting transition temperature on carrier concentration in semiconducting $SrTiO_3$. *Phys. Rev. Lett.* **14,** 305–307 (1965).
40. Pfeiffer, E. R. & Schooley, J. F. Superconducting transition temperatures of Nb-doped $SrTiO_3$. *Phys. Lett.* **29A,** 589–590 (1969).
41. van der Marel, D., van Mechelen, J. L. M. & Mazin, I. I. Common Fermi-liquid origin of T^2 resistivity and superconductivity in n-type $SrTiO_3$. *Phys. Rev. B* **84,** 205111 (2011).
42. Li, L., Richter, C., Mannhart, J. & Ashoori, R. C. Coexistence of magnetic order and two-dimensional superconductivity at $LaAlO_3/SrTiO_3$ interfaces. *Nature Phys.* **7,** 762–766 (2011).
43. Fischer, E. & Hegenbarth, E. Glasslike behaviour of $SrTiO_3$ single-crystal at low temperatures. *Ferroelectrics Lett.* **5,** 21–27 (1985).
44. Viana, R., Lunkenheimer, P., Hemberger, J., Bohmer, R. & Loidl, A. Dielectric spectroscopy in $SrTiO_3$. *Phys. Rev. B* **50,** 601–604 (1994).
45. Uwe, H. & Sakudo, T. Stress-induced ferroelectricity and soft phonon modes in $SrTiO_3$. *Phys. Rev. B* **13,** 271–286 (1976).
46. Yamada, Y. & Shirane, G. Neutron scattering and nature of the soft optical phonon in $SrTiO_3$. *Phys. Soc. Jpn* **26,** 396–403 (1969).
47. Uwe, H. & Sakudo, T. Electrostriction and stress-induced ferroelectricity in $KTaO_3$. *J. Phys. Soc. Jpn* **38,** 183–189 (1975).
48. Shirane, G., Nathans, R. & Minkiewicz, V. J. Temperature dependence of the soft ferroelectric mode in $KTaO_3$. *Phys. Rev.* **157,** 396–399 (1967).
49. Shigenari, T. *et al.* Raman spectra of the ferroelectric phase of $SrTi^{18}O_3$: Symmetry and domains below T_c and the origin of the phase transition. *Phys. Rev. B* **74,** 174121 (2006).
50. Takesada, M., Itoh, M. & Yagi, T. Perfect softening of the ferroelectric mode in the isotope-exchanged strontium titanate of $SrTi^{18}O_3$ studied by light scattering. *Phys. Rev. Lett.* **96,** 227602 (2006).

Acknowledgements

We would like to thank M. A. Carpenter, G. Catalan, P. Chandra, G. Chapline, S. J. Chorley, P. Coleman, G. Conduit, J. P. Griffiths, M. Grosche, C. R. S. Haines, D. E. Khmelnitskii, K. H. Kim, P. B. Littlewood, C. Liu, N. Marcano, N. D. Mathur, N. P. Ong, L. Pálová, C. Panagopoulos, E. Saitovitch, B. D. Simons, D. J. Singh and I. R. Walker for their help and discussions. We would also like to acknowledge support from Emmanuel, Jesus and Trinity colleges of the University of Cambridge, the Engineering and Physical Sciences Research Council (EPSRC grant EP/K012894/1), the European Research Council (ESF) COST P16, the Princeton Center for Complex Materials, IHT KAZATAPROM and the INTELBIOMAT programme.

Author contributions

The findings presented in this paper arose out of a cooperative effort of all the authors, who each played an essential role.

Additional information

Supplementary information is available in the online version of the paper. Reprints and permissions information is available online at www.nature.com/reprints. Correspondence and requests for materials should be addressed to S.E.R., G.G.L. or S.S.S.

Competing financial interests

The authors declare no competing financial interests.